icrrd
Quality Index Research Journal
INTERNATIONAL CENTER FOR RESEARCH AND RESOURCES DEVELOPMENT article
ISSN Number: 2773-5958, SSM Number: (1347468-T), doi.org/10.53272/icrrd, www.icrrd.com

Investigation of on the Tensile Properties of Lnconel 625 Alloy at High Temperature by Activated Tungsten Inert Gas Welding (A-TIG)

J. Sivakumar[1*], Karthik Babu N.B[2], M.P. Mohanraj[3], B. Prabhu[4], E. Hariharan[5], J. Ramesh[6]

[1, 3, 4,5]*Department of Mechanical Engineering, Annapoorana Engineering College Salem – 636308, Tamil Nadu, India*

[2]*Faculty in Department of Mechanical Engineering, Assam Energy Institute, Centre of Rajiv Gandhi Institute of Petroleum Technology, Sivasagar – 785697 - Assam.*

**Corresponding author; Email: jsksivaap@gmail.com*

Received: 12 November 2021 **Accepted:** 23 January 2022
1st Revision: 29 November 2021 **Available Online**: 12 March 2022
2nd Revision: 12 December 2021 **Published:** 12 March 2022
Volume-3, Issue-1 **Cite This:** *ICRRD Qual. Ind. Res. J.* 2022, 3(1), 133-144

ABSTRACT: Activated tungsten inert gas welding (A-TIG) of Inconel 625 with a thickness of 6.5 mm was used as applicant material for investigation in this study. 230 A welding current, 80 mm/min travel speed, and 1 mm arc gap with 2.204 kJ/mm heat input were used to prepare the weld joint. Tensile characteristics were tested at room temperature, 250°C, 450°C, and 650°C. It was clear that with an increase in temperature, ultimate strength and yield strength diminished, while percentage elongation increased. Ultimate tensile strength (UTS) declined nearly 20 percent at temperatures above 650°C compared to UTS at ambient temperature.

Keywords: A-TIG welding, Inconel 625, Tensile strength, Various temperatures.

1. Introduction

Because of its exceptional corrosion resistance and great mechanical qualities, Inconel 625 is utilized in power generation, oil-gas sectors, petrochemical processing, marine engineering, aerospace engineering, and nuclear reactor systems at high temperatures. Because of these properties, Inconel 625 alloys have seen an increase in engineering applications. With the employment of Inconel 625 in nuclear power, aeronautics, oil, gas turbines, and food industries, the welding metallurgy of Inconel 625 has now become a dynamic research area [1, 2]. Elements like chromium and molybdenum present in this superalloy strengthen the metal above a substitutional solid solution. The alloy also contains Al, Nb, and Ti which strengthen it through phases such as MC carbides, M_6C carbides, and $M_{23}C_6$ carbides [3]. Weldability of Inconel 625 is excellent mostly [4]. The weld zone solidifies to result in an austenite matrix with an interdendritically precipitated laves phase [5]. The leading reaction of Inconel 625 in Nb segregation are Niobium carbides which interact with carbon to create Niobium carbides, and the remaining Cr, Nb, and Fe rich molten metal form the Laves phase. The consequences of Niobium carbides on the weld metal have not been studied. However, researchers discovered that lowering the laves phase boosted weldment ductility (Inconel 625). Superalloys Inconel 718 and 625 have similar chemical composition including laves and carbide migration during weld metal solidification [6] . When the cooling rate of Inconel 718 weld zone was increased, Nb segregation was

reduced, and thereafter resulted in Laves phase precipitation. On consuming pulsed current, cooling rate increased which resulted in a decrease in Nb segregation and Laves phase [7]. To reduce the Laves phase in Inconel 718, researchers recommend using weld metal methods. Large thermal gradients, low heat inputs, heat extraction devices, filler metals with low Nb % filler metals, high cooling rates, and pulsed current welding processes are among them [8, 9-10]. TIG welding is widely used to attach components of various thicknesses. On the other hand, TIG welding, makes it difficult to achieve high depth in a single pass [11, 12]. TIG welding of thick components necessitates edge preparation and selection of an appropriate filler wire. Development of deformation and residual stress can affect the mechanical properties of welded components due to the accumulation of a significant temperature gradient [13, 14]. Depth of penetration achievable in a single pass TIG welding methods is the foremost concern. Minimum torch travel motion and filler metal deposition rate jointly lead to poor production [15]. Over the years, detailed investigations have led to the introduction of a variety of techniques to increase penetration depth in traditional TIG operations. Activated flux tungsten inert gas welding (A-TIG) was developed to overcome the limitations of traditional TIG welding [16, 17-18]. A few studies looked at the Marangoni convection effects of Activated flux-TIG welding in a single pass with appropriate input process settings in terms of penetration depth. [19]. Activated flux can be used in the A-TIG process to increase penetration depth without the need of edge preparation [20]. A-TIG welding of Inconel 625 produced a welding connection with less residual stress and deformation. Angular distortion estimations were lower with A-TIG welding. In a single pass, the A-TIG welding process produced excellent weld properties with no weld flaws [21]. An analysis of A-TIG welding with Inconel 625 as the base metal was undertaken to optimize welding process parameters. In relation to other criteria, the data demonstrated the substantial influence played by current. Welding heat input increased with a rise in current. The results also revealed that the flow prevented niobium atoms from migrating. As a result, creation of the laves phase was significantly reduced, resulting in increased penetration depth. To complete the enhanced optimum input parameters for the production of welded joints with appropriate penetration depth, A-TIG welding employs specific optimization approaches such as grey relational analysis [22-23].

A-TIG welding of Inconel 625 alloy was the subject of a thorough literature review. It was noted that less research was available to understand material behaviour at extreme temperatures. Hence this study was initiated to investigate the behaviour of a welded specimen at elevated temperatures.

2 Experimental Technique

2.1 Materials and methods

The base metal used in this study was Inconel 625 plates with a thickness of 6.5 mm. Chemical composition of the base metal was determined using an optical emission spectroscope (OES), with the results shown in Table 1. Indira Gandhi Centre for Atomic Research (IGCAR) at Kalpakkam produced an activated flux for A-TIG welding. Inconel 625 plates were cut to 200 mm x 80 mm x 6.5 mm coupons for A-TIG welding. The machined coupons were wiped and cleaned with acetone to remove stains and surface impurities before being clamped into 25 mm thick copper backer plates. Activated flux was centrifuged using a multicomponent flux with acetone, as shown in Figure 1 (a) with A-TIG welding square butt weld structure 1 (b) and weld pad 1 (c). A thin layer of active flux was added to the weld joint's surface before welding. For a few seconds, the coating was allowed to dry after which, autogenous TIG welding procedures were used on the surface. A Precision TIG 375 welding machine

is shown in Figure 2. The influence of welding process parameters on penetration depth, welding cross sectional area, micro hardness, weld bead width, and weld bead height were determined using a bead on plate trails experiment to discover the optimized input parameters. For A-TIG welding, a 3 mm 2 percent thoriated tungsten electrode with a 60° tip angle was used as shown in Table 2. As a shielding gas, argon was employed at a flow rate of 10 L/min. The activated flux improved TIG welding penetration depth by reversing the Marangoni convection mechanism. The parameters listed in Table 3 were used to produce the weldment.

Table 1: Chemical composition in weight in %

Eleme	C	Si	S	P	Mn	Cr	M0	V	Cu	W	Ti	Co	Al	Nb	Fe	Ni

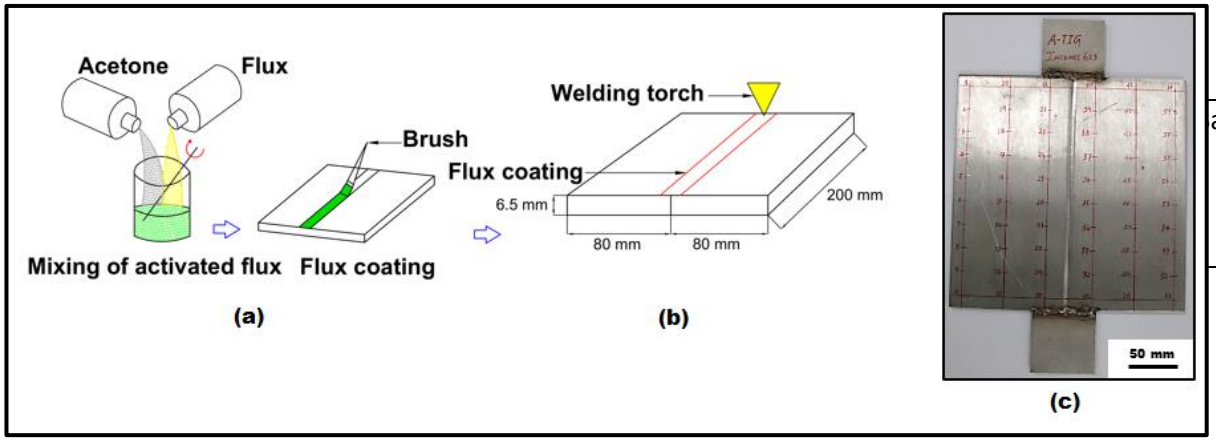

Figure 1 (a): Mixing of multicomponent flux with acetone, (b) A-TIG welding square butt weld structure, (c) weld pad

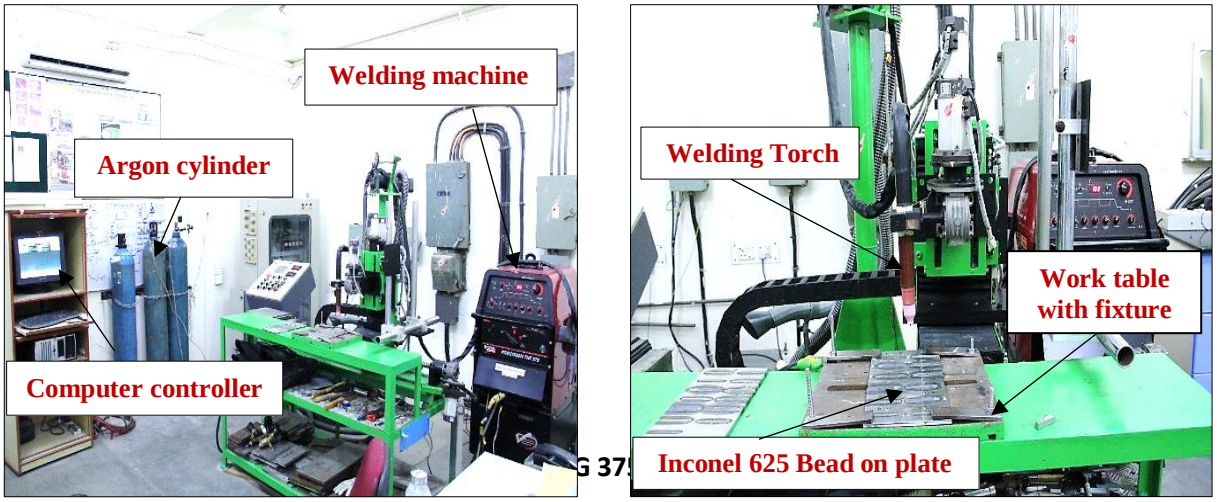

Table 2: Welding Machine Specifications

Table 3: A- TIG welding process parameter

Machine	PRECISION TIG 375 Autogenous welding (Digital TIG Welding Machine)
Polarity	DCEN
Electrode	3mm 2% thoriated tungsten electrode
Electrode Tip angle	60°
Inert gas shielding	Ar (99.99% Purity)
Argon (Ar) gas flow rate	10 lpm
Torch position	Vertical
Cooling	Water cooled torch

Welding current (A)	Voltage (V)	Torch Travel speed (mm/min)	Arc gap (mm)	Heat input (kJ/mm)
230	14.2	80	1	2.204

Tensile test samples were made from transverse weld sections, and the tests performed using a UTM (50 kN load cell) with a nominal loading rate of 1 mm/min as per ASTM: E8/8M standards. For A-TIG and TIG weldments, tensile characteristics such as tensile strength (MPa), yield stress (MPa), and total elongation (percent) were determined. Tensile test was carried out at room temperature set up as shown in Figure 3(a) Universal testing machine set up (b) Sample loaded in the machine (c) Room temperature samples. Figure 4 shows the tensile test at elevated temperatures of 250°C, 450°C, and 650°C equipment. Results of the tensile test at various temperatures are tabulated in Table 4.

Figure 3: Universal testing machine set up (b) Sample loaded in machine (c) Room temperature samples

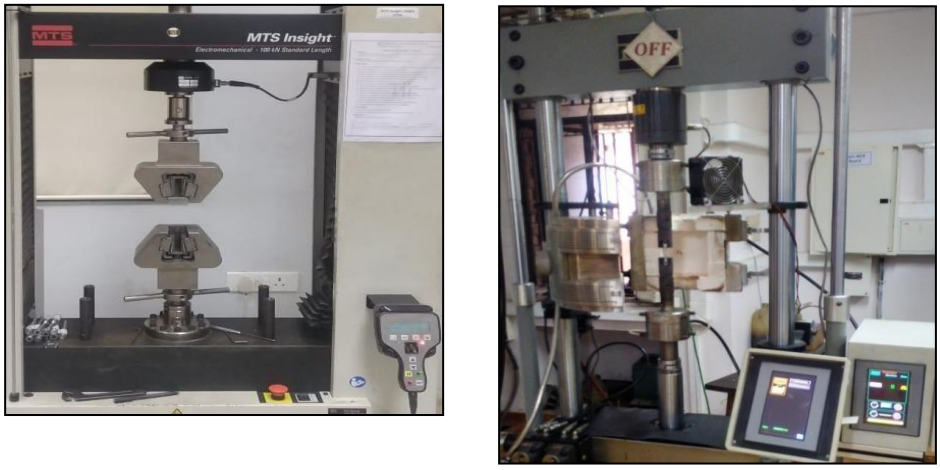

Figure 4: Tensile test at elevated temperature of 250°C, 450°C and 650°C

Table 12: Tensile test results

Type of the specimen	Yield strength, Mpa	Tensile Strength, Mpa	Elongation, %	Fracture locality
A-TIG at Room Temperature	415	881	60.2	Weld metal
A-TIG at 250℃	382	751	44.9	Weld metal
A-TIG at 450℃	380	745	40.5	Weld metal
A-TIG at 650℃	375	740	39.3	Weld metal

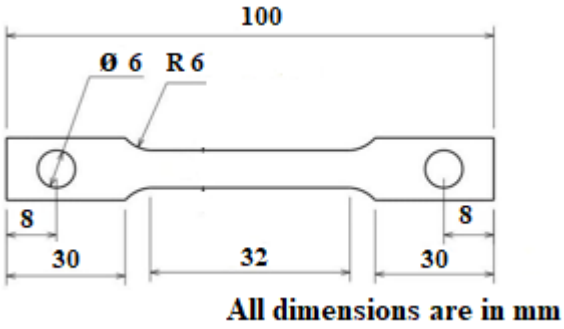

Figure 5: Schematic representation of tensile test sample for various temperature.

3 Effect of tensile properties

As indicated in Figure 5, a schematic representation shows the tensile test specimen of A-TIG welded Inconel 625 plates cut by wire cut EDM according to ASTM E8 standards. Each specimen (pinned specimen) had openings on both ends to allow attachment to the loading shafts at the top and bottom of the UTM and elevated temperature UTM furnaces. These pinned specimens were made to not interfere with the specimen's fracture.

Tensile tests were carried out at room temperature, and at temperatures 250^{0}C, 450^{0}C, and 650^{0}C, respectively. Figure 4 depicts the set-up that was accessible.

Tensile test of an A-TIG welded Inconel 625 specimen was performed at room temperature, and its mechanical properties discovered. The specimen's ultimate tensile strength was determined as 881 MPa, and a fracture seen on the base material. Figure 6 shows the Engineering stress-strain curve of A-TIG welding of Inconel 625 at room temperature.

Figure 9 shows that when the temperature was raised from 25 to 250 degree celsius, both ultimate tensile strength (UTS) and yield strength (YS) decreased along with a gradual increase in reduction area and elongation. It was established that as the temperature increased, both UTS and YS decreased while plastic behaviour improved, which was linked to the merging of the fibrous zone with the radiation area on the tensile fracture surfaces. The specimen's ultimate tensile strength was determined as 751 MPa, and a fracture discovered at the weld zone. Figure 7 shows the Engineering stress-strain curve of A-TIG welding of Inconel 625 at 250°C.

Mechanical property of the base metal testing deteriorated as the temperature increased above 450°C.With increasing temperatures above 450°C, mechanical characteristics of the welded joints also deteriorated. It was also discovered that at 450°C, the welded joint's ductility decreased less. The specimen's ultimate tensile strength was determined as 745 MPa, and a fracture discovered at the weld metal. Figure 8 shows the Engineering stress-strain curve of A-TIG welding of Inconel 625 at 450°C.

It was noticed that as temperature increased above 650°C, tensile strength of the joint decreased and plastic deformation increased. The specimen's ultimate tensile strength was determined as 740 MPa, and a fracture was discovered on the weld material. Figure 9 shows the Engineering stress-strain curve of A-TIG welding of Inconel 625 at 650°C.

Ultimate Force N	Ultimate Stress MPa	Area mm²	Thickness mm	Width mm	Yield Stress MPa	Total Elongation (Auto %
34600	881	39.3	6.45	6.10	415	60.2

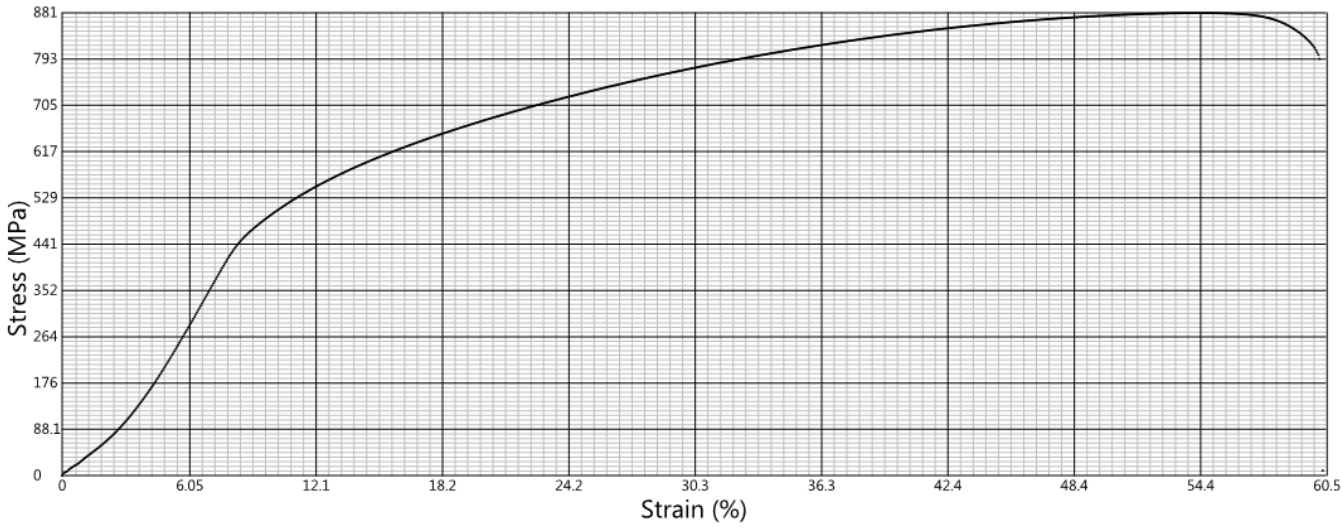

Figure 6: Engineering stress-strain curve of A-TIG welding of Inconel 625 at room temperature

Ultimate Force N	Ultimate Stress MPa	Area mm²	Thickness mm	Width mm	Yield Stress MPa	Total Elongation (Auto %
29400	751	39.1	6.50	6.01	751	44.9

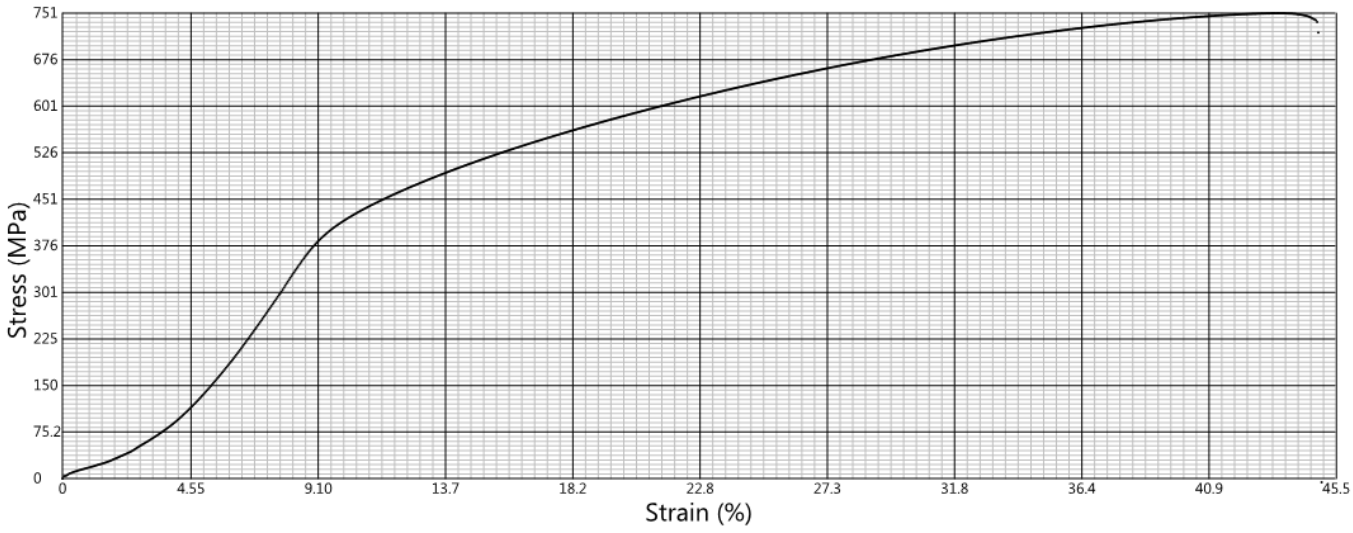

Figure 7: Engineering stress-strain curve of A-TIG welding of Inconel 625 at 250℃

Ultimate Force N	Ultimate Stress MPa	Area mm²	Thickness mm	Width mm	Yield Stress MPa	Total Elongation (Autc %
29100	745	39.1	6.50	6.01	745	40.5

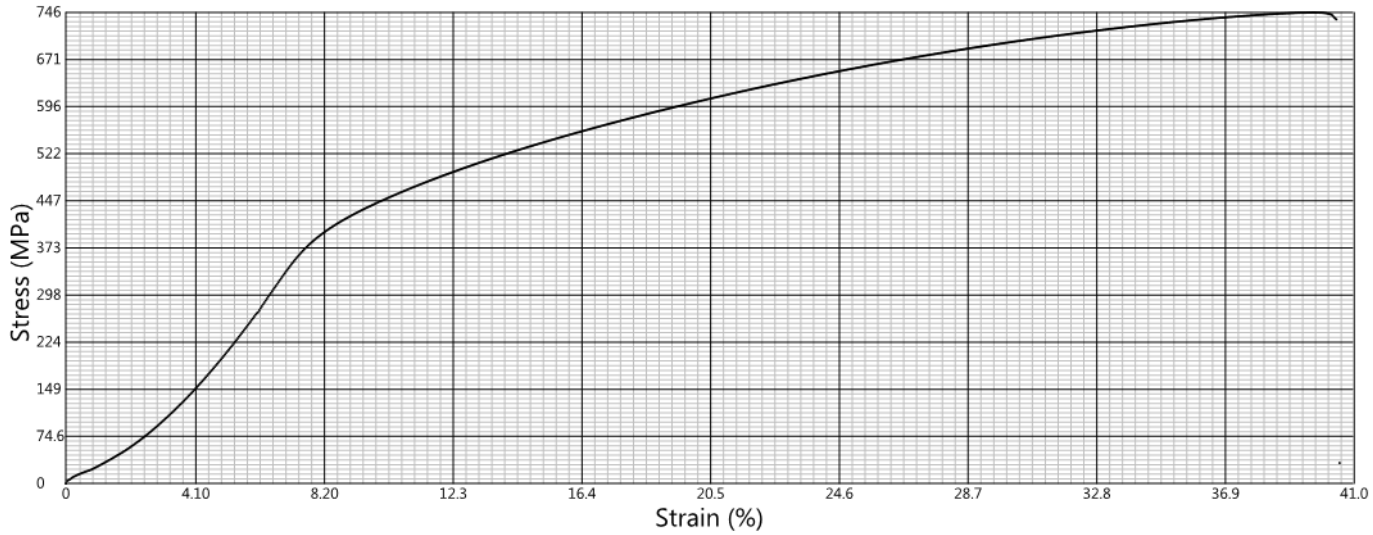

Figure 8: Engineering stress-strain curve of A-TIG welding of Inconel 625 at 450℃

Ultimate Force N	Ultimate Stress MPa	Area mm²	Thickness mm	Width mm	Yield Stress MPa	Total Elongation (Autc %
28700	740	38.8	6.45	6.02	740	39.3

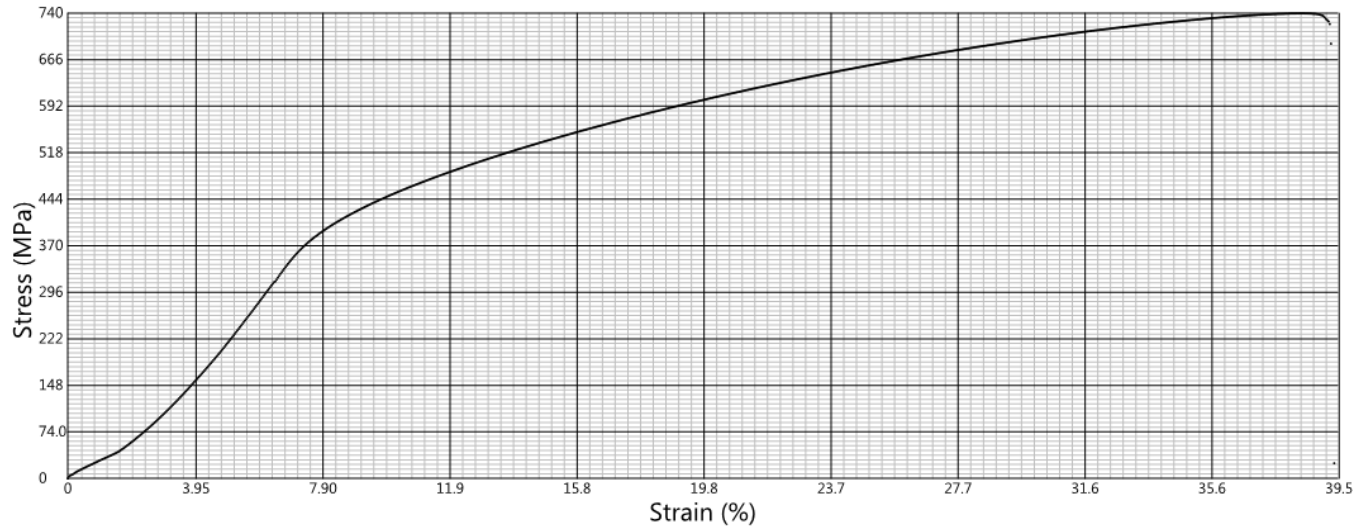

Figure 9: Engineering stress-strain curve of A-TIG welding of Inconel 625 at 650℃

In a single pass, A-TIG welding of Inconel 625 at ambient temperature produced 881 Mpa, whereas A-TIG welding at 250°C produced 751 Mpa. At 450°C, the pressure was 745 Mpa, and at 650°C, 740 Mpa. According to the findings, A-TIG weldment showed a higher tensile strength at room temperature but lower tensile strength than at ambient temperature due to finer microstructure.

This could be because a partially melted zone was formed (PMZ). Formation of PMZ could result in a loss of strength and ductility. In addition, increased heat input was linked to extensive liquation of

grain borders and coarse grain structure inside PMZ. The presence of a partially melted zone explains the different tensile behaviours.

A-TIG weldment's decreased tensile strength resulted in lower percentage elongation. Due to ductile mode failure, voids and dimples were readily visible. Because of the segregation of Nb and Mo precipitates in the dendritic areas and coarser grain structure, A-TIG weldment showed a poor tensile strength at ambient temperature. The weld techniques showed voids, dimple facets, and shear rupture. Because cleavage and crack boundary were not visible, the tensile fractography of the Inconel 625 welding procedures exhibited a ductile fracture mode. This could be due to the existence of secondary phases in the dendrites and inter-dendritic areas of A-TIG weldments. In the inter-dendritic regions, findings of microstructure investigations and depletion of Mo, Cr, and Nb in the fusion zones of both weldments were separated. In the fusion zone, the laves phase was visible at grain boundaries, resulting in the main impact of crack growth. Without any solidification cracking, migrating grain boundaries were formed by utilizing both welding procedures. Increased Nb rich secondary phases in the A-TIG welding fusion zone contributed to a lower tensile strength.

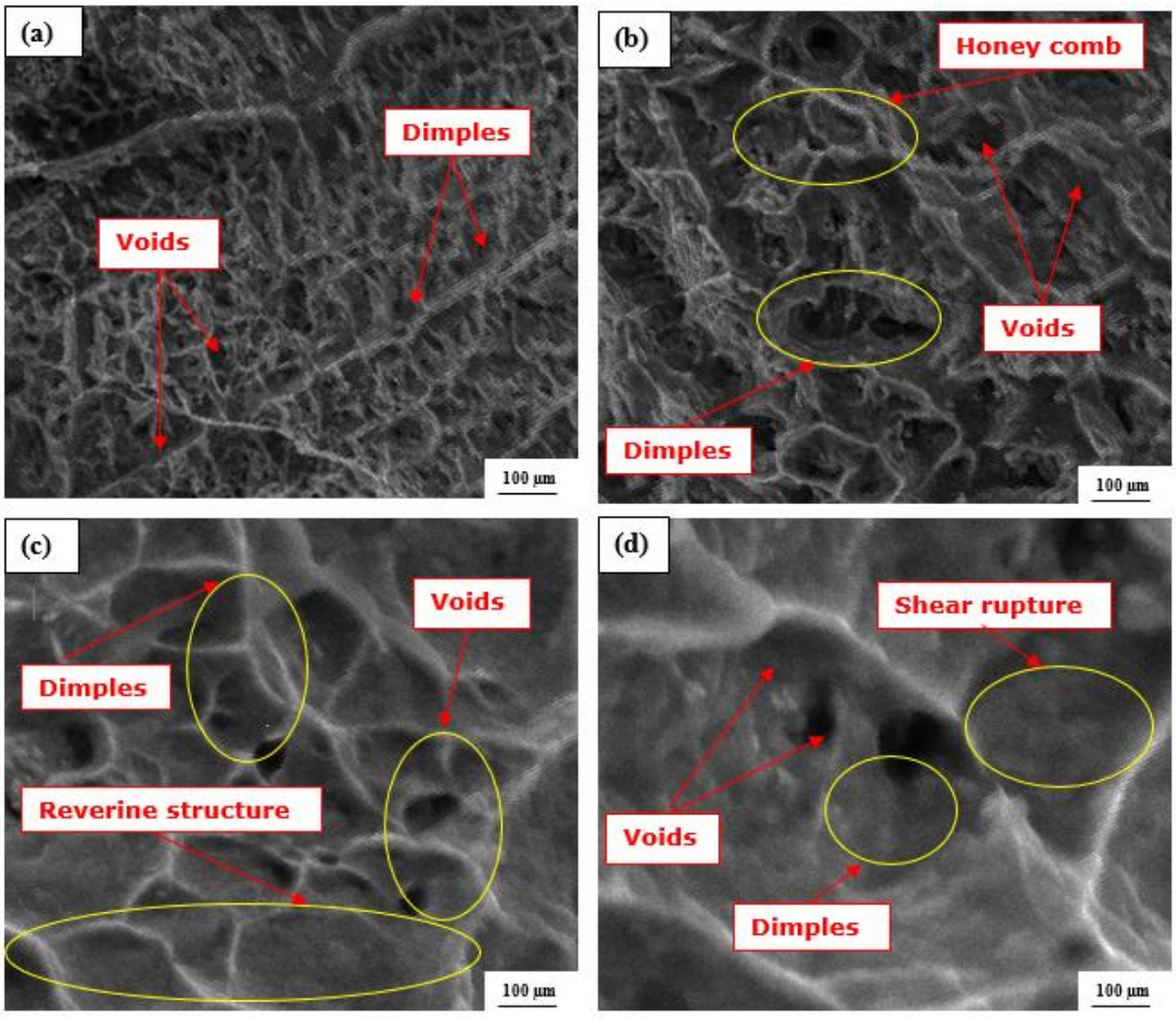

Figure 10: SEM fractography of the A-TIG weld joint (a) Room temperature (b) at 250°C (c) at 450°C (d) at 650°C (Tensile test)

On the ductile fracture surface, high magnification under microscope revealed the creation of a honeycomb with many spherical dimples separated by thin walls. This showed that many holes were formed on the surface separated by thin walls until they fractured. Dimples generated in the cup's shear lip and the cone fracture will grow longer until they reach a parabolic shape, thus indicating shear failure.

4 Conclusion

Precision 375 TIG welding equipment was used to conduct A-TIG welding experiments on Inconel 625 alloy. Mechanical testing was carried out at both elevated and ambient temperatures and the following are the conclusion:

At room temperature, the welded specimen's ultimate tensile strength was 881 MPa, and failure was determined at the weld zone. Tensile strength of 751 Mpa was observed for Inconel 625 by A-TIG welding at 250°C, 745 Mpa at 450°C, and 740 Mpa at 650°C

Because of the segregation of Nb and Mo precipitates in the dendritic areas and coarser grain structure, A-TIG weldment showed a poor tensile strength at ambient temperature. The weld techniques showed voids, dimple facets, and shear rupture. As cleavage and crack boundary were not visible, tensile fractography of Inconel 625 welding procedures exhibited a ductile fracture mode. This could be due to the existence of secondary phases in the dendrites and inter-dendritic areas of A-TIG weldments.

It is clear that as temperature rises, ultimate strength and yield strength drop along with percentage of elongation. The ultimate tensile strength (UTS) decreased roughly 20 percent at temperatures above 650°C, compared to UTS at ambient temperature.

CONFLICTS OF INTEREST

There are no conflicts to declare.

REFERENCES

1. Special metals corporation products: INCONEL® alloy 625, www.specialmetals.com/products.

2. Dinda GP, Dasgupta AK, Mazumder J et al (2009) Laser aided direct metal deposition of Inconel 625 superalloy: Microstructural evolution and thermal stability. Material Science and engineering A 509(1-2):98-104.

3. Xu LY, Jing HY, Han YD et al (2018) Effect of welding on the corrosion behavior of X65/Inconel 625 in simulated solution. Welding in the World 62(2):363-375.

4. Xing X, Di X, Wang B et al (2014) The effect of post-weld heat treatment temperature on the microstructure of Inconel 625 deposited metal. Journal of Alloys and Compounds 593:110-116.

5. Dupont JN, Lippold JC, Kiser SD et al (2005) Welding metallurgy and weldability of nickel alloys. Hoboken (NJ): John Wiley & Sons.

6. Cieslak MJ, Headley TJ, Romig AD, Kollie T et al (1988) A melting and solidification study of alloy 625. Metallurgical Transactions A 19(9):2319-31.

7. Tumer M, Karahan T, Mert T et al (2020) Evaluation of microstructural and mechanical properties of dissimilar Inconel 625 nickel alloy– UNS S32205 duplex stainless steel weldment using MIG welding. Welding in the World 64:21–35.

8. *Floreen S, Fuchs GE, Yang WJ et al (1994)* The Metallurgy of Alloy *625*. The Minerals, Metals & Materials Society *13–37*.

9. Manikandan SG, Sivakumar D, Rao KP, Kamaraj M et al (2014) Effect of weld cooling rate on Laves phase formation in Inconel 718 fusion zone. Journal of Materials Processing Technology 214(2):358-64.

10. Ramkumar KD, Kumar BM, Krishnan MG, Dev S, Bhalodi AJ, Arivazhagan N, Narayanan S et al (2015) Studies on the weldability, microstructure and mechanical properties of activated flux TIG weldments of Inconel 718. Materials Science and Engineering: A 639:234-44.

11. Radhakrishna CH, Rao KP (1997) The formation and control of Laves phase in superalloy 718 welds. Journal of Materials Science 32(8):1977-84.

12. S. Kou, Welding metallurgy (2003) New Jersey, USA 431-446.

13. Tumer M, Mert T, Karahan T et al (2020) Investigation of microstructure, mechanical, and corrosion behavior of nickel-based alloy 625/duplex stainless steel UNS S32205 dissimilar weldments using ERNiCrMo-3 filler metal. Welding in the World pp.1-12.

14. Howse DS, Lucas W (2000) Investigation into arc constriction by active fluxes for tungsten inert gas welding, Science and Technology of Welding and Joining 5(3):189-193.

15. Deng D, Murakawa H (2006) Numerical simulation of temperature field and residual stress in multi-pass welds in stainless steel pipe and comparison with experimental measurements. Computational materials Science 37(3):269-77.

16. Vasudevan M (2007) Computational and experimental studies on arc welded austenitic stainless steels [PhD Thesis] Indian Institute of Technology, Chennai.

17. Vasantharaja P, Maduarimuthu V, Vasudevan M, Palanichamy P et al (2012) Assessment of residual stresses and distortion in stainless steel weld joints. Materials and Manufacturing Processes 27(12):1376-81.

18. Sakthivel T, Vasudevan M, Laha K, Parameswaran P, Chandravathi KS, Mathew MD, Bhaduri AK et al (2011) Comparison of creep rupture behaviour of type 316L (N) austenitic stainless steel joints welded by TIG and activated TIG welding processes. Materials Science and Engineering A 528(22-23):6971-80.

19. Pandey C, Mohan Mahapatra M, Kumar P, Saini N et al (2018) Autogenous tungsten inert gas and gas tungsten arc with filler welding of dissimilar P91 and P92 steels. Journal of Pressure Vessel Technology 140 (2).

20. Sivakumar J, Korra NN, Vasantharaja P. (2020) Computation of residual stresses, distortion, and thermogravimetric analysis of Inconel 625 weld joints. Proceedings of the Institution of Mechanical Engineers, Part C: J of Mech Eng Sci. 1-10.

21. Sivakumar J, Vasudevan M, Korra NN. (2020) Systematic Welding Process Parameter Optimization in Activated Tungsten Inert Gas (A-TIG) Welding of Inconel Transactions of the Indian Institute of Metals. 73:555-569.

22. Sivakumar, J, Naik, K.N (2020) Optimization of weldment in bead on plate welding of nickel based superalloy using Activated flux tungsten inert gas welding (A-TIG). Mater Today Proc. 27: 2718-2723.

23. Sivakumar, J., Vasudevan, M. & Korra, (2021) N.N. Effect of activated flux tungsten inert gas (A-TIG) welding on the mechanical properties and the metallurgical and corrosion Assessment of Inconel 625. Weld World 65, 1061–1077.

24. Sivakumar, J., and Nanda Naik Korra. (2021) Optimization of Welding Process Parameters for Activated tungsten inert welding of Inconel 625 using Technique for Science and engineering, Arabian Journal for Science and Engineering.1-11.